Linear and Nonlinear Electro-optic Response of MHPOCBC

Andika Fajar[1,*] & Hiroshi Orihara[2]

[1]Research Center for Nanotechnology System, National Research and Innovation Agency, KST. B.J. Habibie, Jalan Raya Puspiptek 60, South Tangerang 15314, Indonesia
[2]Research Institute for Electronic Science, Hokkaido University, N20W10 Kita-Ward Sapporo 001-0020, Japan
[*]E-mail: andi009@brin.go.id

Abstract. This study investigated the linear and second-order electro-optic responses in chiral smectic liquid crystal 4-(1-methylheptyloxycarbonyl) phenyl 4-octylcarbonyloxybiphenyl-4-carboxylate (MHPOCBC). The result revealed a single Debye-type relaxation in the linear electro-optic frequency dispersion, with a relaxation frequency extending up to one hundred kHz. Conversely, the second-order electro-optic response exhibited intricate temperature-dependence, accurately depicted by a phenomenological Landau theory around the SmA–SmC_α* phase transition point. Notably, in the SmC_α* phase, critical slowing down of the amplitude mode occurred near the transition to the SmA phase, while at lower temperatures of the SmC_α* phase, a distinct low-frequency relaxation mode emerged. Furthermore, the relaxation frequency of the antiferroelectric Goldstone mode in the SmC_A* phase remained constant across the entire temperature range. These findings should significantly contribute to the understanding of dynamic behaviors in chiral smectic liquid crystals, shedding light on their complex phase transitions and electro-optic properties.

Keywords: *chiral smectic; electro-optic; liquid crystal; relaxation mode; MHPOCBC.*

1 Introduction

Previous dynamical behavior investigations of chiral smectic liquid crystals under an AC electric field to explore their response to external stimuli involved dielectric and electro-optic measurements [1-3]. While the conventional method uses AC electric fields to observe the frequency dispersion, both approaches typically operate within a linear framework. Owing to the inherent substantial softness in liquid crystals, their response to external fields readily exhibits nonlinear behavior. Both measurements are extended into the nonlinear regime to capture these complexities, offering more detailed insight into the dynamics of chiral smectic liquid crystals. In contrast to dielectric measurements, the electro-

Received February 19th, 2024, Revised April 19th, 2024, Accepted for publication April 22nd, 2024
 ISSN: 2337-5760, DOI: 10.5614/j.math.fund.sci.2024.55.3.2

optic method is anticipated to be less affected by sample DC conductivity and can be adjusted to various cell configurations due to its optical nature. Second-order electro-optic measurement has emerged as a robust approach for observing nonpolar orientational fluctuations, offering insight that is inaccessible through linear spectra [4-9].

The intermediate phase of chiral smectic liquid crystals, smectic C_α* (SmC_α*), has garnered attention owing to its distinctive physical properties [10-12]. This phase appears at temperatures lower than the paraelectric SmA phase. The SmC_α* phase undergoes a transition to the antiferroelectric SmC_A* phase, the ferroelectric SmC* phase, or the ferrielectric phase. Regardless of the sequence of phase transitions, liquid crystals that have this phase always have the SmC_A* phase at temperatures below it. Similar to the SmC* phase, the liquid crystal molecules in the SmC_α* phase form a helical configuration with a helical axis perpendicular to the smectic layer plane, however, the helical pitch is much shorter than that of SmC* [13,14]. It originates from the condensation of a soft mode located at a general point within the SmA phase's smectic Brillouin zone. Therefore, it cannot be detected by conventional methods such as linear dielectric, electro-optic, and dynamic light scattering measurements.

When examining the physical characteristics of the SmC_α* phase, MHPOCBC is one of the chiral smectic crystals of interest. This liquid crystal exhibits a broad temperature range of the SmC_α* phase and a straightforward transition to the SmC_A* phase. A comprehensive exploration of the dynamics surrounding the SmA–SmC_α* phase transition of MHPOCBC has been conducted, utilizing both nonlinear electro-optic [15,16] and dielectric measurements [17-19]. While third-order nonlinear dielectric measurement has revealed the soft mode in the SmA phase [17], its detection using nonlinear electro-optic measurements remains unexplored. Nevertheless, second-order nonlinear electro-optic measurement has revealed softening of the amplitude mode (spatially nonuniform tilting without macroscopic polarization) within the SmC_α* phase alongside the ferroelectric mode [15], which cannot be detected by the linear one.

Thereafter, it has been reported that the low temperature region of the SmC_α* phase exhibits a field-induced phase transition, and that dielectric permittivity hysteresis is present with cooling and heating observations [20-22]. However, there is still a need for a comprehensive exploration of the dynamic properties within the SmC_α* phase. This study aimed to address this gap by conducting linear (first-order) and second-order nonlinear electro-optic measurements in the chiral smectic phases of MHPOCBC, with a particular focus on the lower temperature region of the SmC_α* phase. The objective was to provide comprehensive insight into the dynamic properties of this chiral smectic liquid

crystal by using the information obtained by linear and nonlinear electro-optic response measurements. The following sections will present a brief overview of electro-optic effect expressions in the SmC_α* phase, followed by detailed discussions on the experimental setup and results.

2 Electro-optic Response in the Chiral Smectic Phases

The transmitted light intensity I in electro-optic measurements for a homogeneous cell, positioned between the perpendicular polarizer and the analyzer configuration, can be represented as follows [23,24]:

$$\frac{I}{I_0} = \sin^2(2\alpha)\sin^2(\beta n_a) \tag{1}$$

where $\beta = \pi d/\lambda$ and I_0 represents the incident light intensity. This expression incorporates parameters such as α (the angle between an indicatrix principal axis and the polarizer direction), β (related to the cell gap, d, and incident light wavelength, λ), and n_a (refractive index anisotropy). The relaxation modes induced by an electric field $E = E_0 \cos \omega t$ modify both α and n_a as follows:

$$\alpha = \alpha_0 + \Delta\alpha \tag{2a}$$

$$n_a = n_{a0} + \Delta n_a \tag{2b}$$

Here, α_0 and n_{a0} represent equilibrium values without an external field, while $\Delta\alpha$ and Δn_a describe the induced changes due to the electric field. The expression for the transmitted light intensity change, ΔI, caused by an applied electric field [23,25], obtained by substituting Eq. (2) into Eq. (1), is:

$$\frac{\Delta I}{I_0} = 2\sin 4\alpha_0 \sin^2(\beta n_{a0})\,\Delta\alpha + 4\cos 4\alpha_0 \sin^2(\beta n_{a0})\,\Delta\alpha^2 +$$

$$\beta \sin^2 2\alpha_0 \sin(2\beta n_{a0})\,\Delta n_a. \tag{3}$$

Since $\Delta\alpha$ and Δn_a are directly related to the electric field and its square, the linear electro-optic response captures the observable influence of the initial term in Eq. (3). Conversely, the subsequent two terms can be observed within the second-order response.

A prior study established a phenomenological theory concerning the second-order electro-optic response within the SmC_α* phase under AC fields, deriving relevant equations [15]. The components induced by the field in Eq. (1), namely $\Delta\alpha$ and Δn_a, are expressed in Eq. (4a) and (4b):

$$\Delta n_a = -\frac{\varepsilon_a}{2}\left(\frac{2}{\sqrt{\varepsilon_\parallel}}+\frac{1}{\sqrt{\varepsilon_\perp}}\right)\xi_s\Delta\xi_1 + \frac{3\varepsilon_a}{4}\left(\frac{1}{\sqrt{\varepsilon_\parallel}}+\frac{1}{\sqrt{\varepsilon_\perp}}\right)\xi_s^2\xi_{fx}^2 \tag{4a}$$

$$\Delta\alpha = \varepsilon_a\xi_{fx} \tag{4b}$$

Incorporating the dielectric coefficient parallel to the molecule axis, $\varepsilon_\parallel$, and the perpendicular, $\varepsilon_\perp$, as well as the dielectric anisotropy, $\varepsilon_a = \varepsilon_\parallel - \varepsilon_\perp$, the spontaneous order parameter, ξ_s, and modes like the ferroelectric mode ξ_{fx} and the amplitude mode $\Delta\xi_1$, these relaxation modes are characterized as in Eq. (5a) and (5b):

$$\xi_{fx} = \mathrm{Re}\left[\chi_f(\omega)e^{i\omega t}\right]cE_0\ , \tag{5a}$$

$$\Delta\xi_1 = \mathrm{Re}\left[\chi_s(2\omega)\left(\frac{\varepsilon_a'}{4}-\frac{1}{2}\lambda c^2\chi_f(\omega)^2\right)e^{i2\omega t}\right]\xi_s E_0^2\ , \tag{5b}$$

where $\chi_f(\omega) = (a+\lambda\xi_s^2+i\omega\gamma)^{-1}$ and $\chi_s(\omega) = (\alpha+3\beta\xi_s^2+i\omega\gamma)^{-1}$ denote the susceptibilities corresponding to the ferroelectric and amplitude modes, respectively, both following a Debye-type relaxation. These modes, related to ferroelectric and amplitude responses, exhibit different behavior concerning the applied field's linearity and square dependence.

The analysis of electro-optic responses in the SmC_α* phase requires understanding Eq. (3). Each term in the equation corresponds to distinct physical effects. The initial term signifies the tilt caused by the electric field (Pockels effect), the subsequent term scales with the field square (related to the ferroelectric mode), and the third term, also field-square dependent, involves contributions from both amplitude and ferroelectric modes (known as the Kerr effect). The interpretation of results derived from these electro-optic responses in the SmCα* phase relies on comprehending these effects.

3 Experimental Setup

The chiral smectic liquid crystal used in the experiment, 4-(1-methyl-heptyloxycarbonyl) phenyl 4-octylcarbonyloxybiphenyl-4-carboxylate (MHPOCBC), exhibited a phase sequence of crystal–SmI_A*–SmC_A*–SmC_α*–SmA–isotropic [26]. The process involved introducing the sample into a homogeneous cell (EHC) with polyimide layers and indium tin oxide (ITO) electrodes. The sample was cooled under controlled conditions from the isotropic phase to the SmA phase. The cell had a gap of approximately 25 μm, with electrodes of an area of 4×4 mm2 each. To improve the sample's alignment, it was exposed to a low-frequency AC electric field for a few hours in the SmA

phase near the SmC_α* phase transition point. The cell was set up on an Instec HS1 hot stage and then placed on an Olympus BH-2 polarizing microscope stage, exposed to light from an argon ion laser (Spectra-Physics, Model 161B) emitting at a wavelength of 488 nm. The smectic layer was subjected to a sinusoidal electric field. The polarizer direction was adjusted to $\alpha_0 = 22.5°$ off from the optical axis between crossed polarizers. In this configuration, the linear and second-order electro-optic responses should detect solely the change in the optical axis ($\Delta\alpha$, related to the Pockels effect) and the alteration in birefringence (Δn_a, corresponding to the Kerr effect) as defined in Eq.(3). A photodiode (Hamamatsu Photonics, C63867) attached to the polarizing microscope was used to record the light that was transmitted. The signal was simultaneously measured using a vector signal analyzer (HP89410), which allowed for the simultaneous determination of the linear and second-order responses' amplitude and phase.

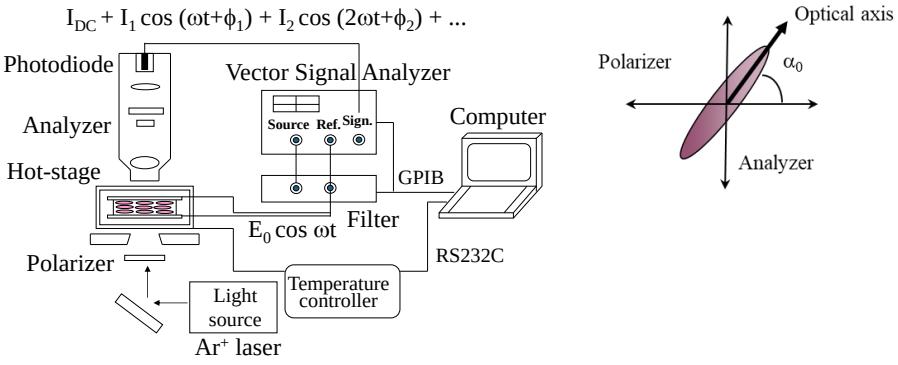

Figure 1 (a) Setup of the linear and second-order electro-optic measurement system and (b) representation of α_0, the angle between the optical axis of the sample and the crossed polarizer-analyzer.

Figure 1 outlines the setup of the electro-optic measurement system, encompassing both linear and nonlinear aspects, in addition to the sample configuration. The complex light intensity ΔI was characterized as follows: $\Delta I = ae^{i\phi}$, where a and ϕ represent the response's amplitude and phase. The real and imaginary parts of electro-optic responses were determined from the obtained amplitude and phase as in Eq. (6a) and (6b):

$$\mathrm{Re}(\Delta I_n) = \frac{V_n}{V_i^n}\cos(\phi_n - n\phi_i) \tag{6a}$$

$$\mathrm{Im}(\Delta I_n) = \frac{V_n}{V_i^n}\sin(\phi_n - n\phi_i) \tag{6b}$$

Here, V_i and ϕ_i represent the applied voltage and phase, respectively, and V_n and ϕ_n for the n-order electro-optic response's output voltage and phase. Frequency variations were assessed across a controlled temperature range from 100 Hz to 1 MHz while maintaining stability.

4 Results and Discussion

The amplitudes of the linear and second-order electro-optic responses of the MHPOCBC during the cooling process are shown in Figure 2 as a function of temperature, measured at 1 kHz with steps of 0.05°C. These profiles display three different temperature areas that decrease in temperature sequentially, corresponding to the SmA, SmC_α*, and SmC_A* phases.

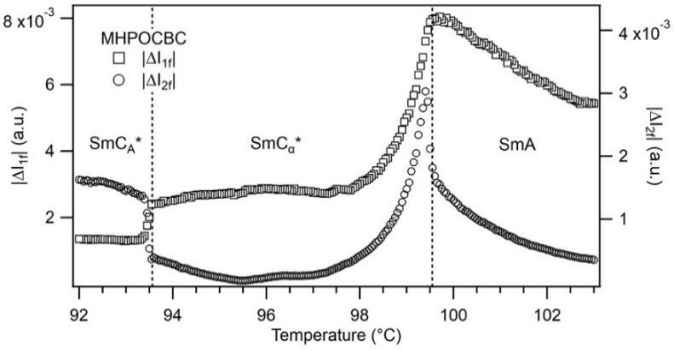

Figure 2 Temperature dependences of the amplitudes of the linear |ΔI1f|, and the second-order, |ΔI2f|, electro-optic response of the MHPOCBC recorded concurrently at 1 kHz during the cooling process.

In both the linear and the second-order electro-optic responses, distinct peaks emerged in the SmA–SmC_α* phase transition area, albeit in a slightly different position. The transition temperature delineating these phases aligned with the peak observed in the linear electro-optic response, as confirmed by detailed simultaneous electro-optical measurements of harmonic and DC signals [27].

Observations within the SmA phase revealed a gradual rise in the linear electro-optic response nearing the transition point, culminating in a peak, followed by a decline within the SmC_α* phase. Previous research highlighted a direct correlation between the linear electro-optic response and the ferroelectric mode susceptibility [15]. As a result, the observed gradual increase in the SmA phase with temperature decreases suggests a partial softening of the ferroelectric mode. Further elaboration of the observation will be provided later.

The linear electro-optic response sharply decreases at lower temperatures during the shift to the SmC_A* phase, distinctly marking this transition point and maintaining an almost constant value afterwards. These SmA–SmC_α* and the SmC_α*–SmC_A* transition points were additionally corroborated by breakpoints evident in the temperature-dependent frequency relaxation of the ferroelectric mode, as elucidated below. The linear electro-optic response demonstrated continuous changes around the SmA–SmC_α* phase transition, whereas a discernible jump was observed during the SmC_α*–SmC_A* phase transition. These results imply that the phase transition at higher temperatures exhibits second-order characteristics, contrasting with the first-order transition at lower temperatures.

Conversely, the temperature-dependent behavior of intensity in the second-order electro-optic response revealed a complex pattern. It showed an elevation through the SmA phase, continuing its ascent throughout the SmC_α* phase, reaching a distinct peak slightly beneath the transition point. This significant increase in the SmC_α* phase may be attributed to the emergence of the spontaneous order parameter value, as highlighted in earlier studies [16]. The amplitude of the second-order electro-optic response reduced with decreasing temperature in the SmC_α* phase, reaching a minimum in the mid-region before ascending until the SmC_A* phase's transition point. The second-order response exhibited a rise at the transition point and remained constant as the temperature decreased.

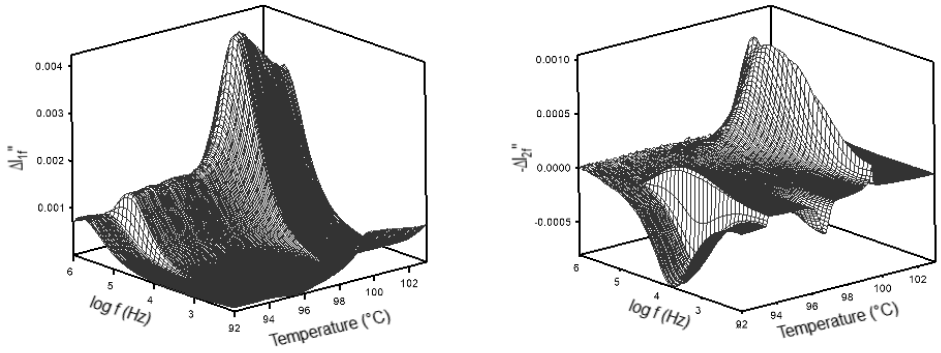

(a) (b)

Figure 3 Temperature dependencies of the imaginary parts for (a) the linear electro-optic frequency dispersion $\Delta I_{1f}''(\omega)$ and (b) the second-order electro-optic frequency dispersion $-\Delta I_{2f}''(\omega)$.

Figure 3 displays the temperature-dependent trends of the imaginary component in the frequency dispersion of both linear and second-order electro-optic responses throughout the cooling process. In Figure 3(a), a single relaxation process is evident solely within the linear electro-optic response, $\Delta I_{1f}"(\omega)$, sustaining across the measured frequency spectrum and diverse temperature ranges in all phases. The observed peak in this response notably corresponds to the ferroelectric mode relaxation frequency, characterized by a homogeneous tilting mode that produces macroscopic polarization.

Figure 3(b) shows the frequency dispersion of the second-order electro-optic response. The peaks on the high temperature side of the SmC_α* phase correspond to the soft mode and amplitude mode that induce the SmA–SmC_α* phase transition, as was previously described in [15]. The peak frequency rose with decreasing temperature, but it started to gradually fall with decreasing peak intensity. When moving to the low temperature side, two new mode peaks were observed. One is the peak close to the SmC_α*–SmC_A* phase transition point. In the midst of the SmC_α* phase, on the low frequency side, is the second mode.

However, since these peaks are connected, they may be in the same mode. Transitioning into the SmC_A* phase, a distinctive Debye-type relaxation mode becomes apparent. The peak frequency remains constant within the measured temperature range. The relaxation process is attributed to the antiferroelectric Goldstone mode, which is unattainable through typical linear dielectric measurements [21] but has been observed in both homogeneous [7] and homeotropic (free-standing film) cells [4] of MHPOBC using second-order electro-optic response.

Figure 4 shows the frequency dispersions of the second-order ΔI_{2f} and the linear ΔI_{1f} electro-optic responses close to the SmA–SmC_α* phase transition temperature of the MHPOCBC. The linear response ΔI_{1f} in both the SmA phase ($T = 99.80$℃) and the SmC_α* phase high-temperature zone ($T = 99.45$℃) exhibits Debye-type relaxations. As specified in Eq. (4), these relaxations are attributed to the ferroelectric mode. The solid line denotes the optimal fitting achieved through Eq. (7):

$$\Delta I_{1f}(\omega) = \frac{A_f}{1+i\omega\tau_f} \tag{7}$$

where $\tau_f = \gamma/(a + \lambda\xi_s^2)$ represents the ferroelectric mode relaxation time. Parameter A_f is related to the ferroelectric mode.

On the other hand, the second-order electro-optic response, ΔI_{2f}, depicted in Figure 4, demonstrated an unexpected Debye-type relaxation attributed to the birefringence change Δn_a detailed in Equation (3). Despite the absence of a Kerr effect in the SmA phase due to the incapacity of an electric field to induce the order parameter ($\xi_s = 0$ from Equation (4)), the presence of small SmC_α* phase clusters, induced by thermal fluctuations within a very narrow temperature range above the transition point, allows for the observation of frequency dispersion induced by these fluctuations [27-29]. Nevertheless, this Debye-type dispersion with a high relaxation frequency is observable across all experimental temperature ranges. These results may stem from irregularities in the orientation of the liquid crystal molecules illuminated by the laser, prompting the emergence and dominance of the second term in Eq.(3), namely the ferroelectric mode, in this experiment. According to Eqs. (3) and (4), the second-order electro-optic response in the SmA phase is fitted with a squared Debye expression in Eq. (8):

$$\Delta I_{2f}(\omega) = \frac{A_f}{\left(1+i\omega\tau_f\right)^2} \tag{8}$$

This confirms the identical ferroelectric mode relaxation frequencies determined from both the linear and second-order responses.

On the other hand, the second-order response within the SmC_α* phase (Figure 4(b)) highlights a notably different frequency dispersion curve than the first-order response. Here, an additional relaxation mode, associated with the soft (amplitude) mode, emerged in the low-frequency domain concerning the SmA-SmC_α* phase transition. Eqs. (4) and (5) demonstrate that the frequency dispersion in the SmC_α* can be examined using the formula:

$$\Delta I_{2f}(\omega) = \frac{1}{1+i2\omega\tau_s}\left(A_{s1} + \frac{A_{s2}}{\left(1+i\omega\tau_f\right)^2}\right) + \frac{A_{f2}}{\left(1+i\omega\tau_f\right)^2} \tag{9}$$

where $\tau_s = \gamma/(a + 3\beta\xi_s^2)$ represents the amplitude mode relaxation time and A_{s1}, A_{s2}, and A_{f2} are adjustable parameters. The amplitude mode is associated with the parameters A_{s1} and A_{s2}, which have their origins in the dielectric anisotropy and the nonlinear coupling between the amplitude mode and the ferroelectric mode, respectively [23]. The value A_{f2} is related to the ferroelectric mode. Eq.(9) was used to analyze the ΔI_{2f} frequency dispersion, which is shown by the solid line in Figure 4(b). This result shows that the experimental data and the theoretical predictions corresponded well. Notably, in the fitting process, τ_f remained fixed at the value determined from the linear response.

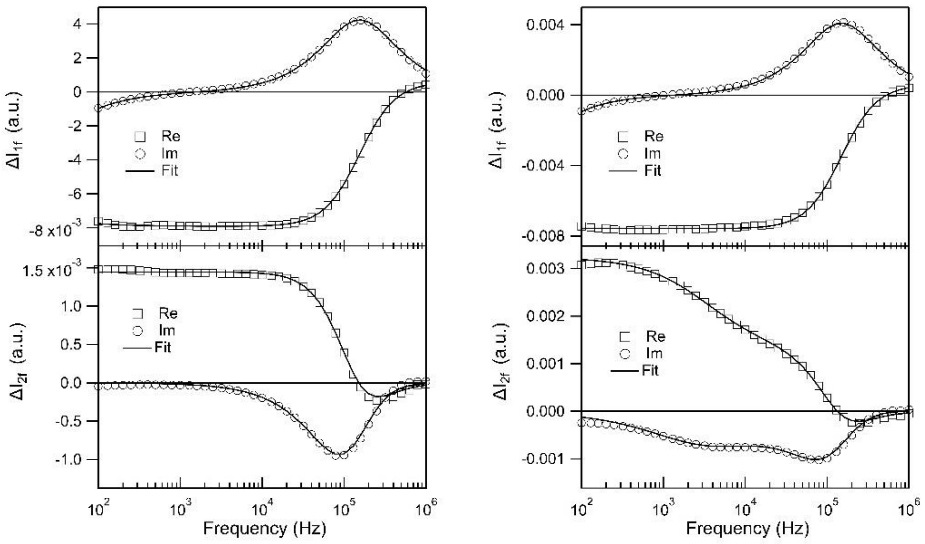

(a) (b)

Figure 4 Frequency dispersions of the linear ΔI_{1f} and the second-order ΔI_{2f} responses within (a) the SmA phase at a temperature of 99.80 ℃, and (b) the high-temperature region of the SmC$_\alpha$* phase at a temperature of 99.45 ℃.

The frequency dispersions of the second-order ΔI_{2f} and the linear ΔI_{1f} electro-optic responses in the middle and low-temperature regions of the SmC$_\alpha$* phase are shown in Figure 5. The linear electro-optic responses ΔI_{1f} exhibited a Debye-type relaxation, as illustrated in Figure 5(a) and Figure 5(b), and were fitted by Equation (7). On the other hand, the second-order responses ΔI_{2f} showed sign inversions and low-frequency mode in both frequency dispersions, as depicted in Figures 5(a) and 5(b). Equation (9) was used to analyze the frequency dispersions. The best-fit results are shown by the solid lines in both figures.

Figure 6 depicts the frequency dispersions of the second-order ΔI_{2f} and the linear ΔI_{1f} electro-optic responses in the SmC$_A$* phase. Figure 6(a) illustrates a Debye-type frequency dispersion in the linear electro-optic response associated with the ferroelectric mode. This dispersion exhibited a higher relaxation frequency compared to the SmA and SmC$_\alpha$* phases.

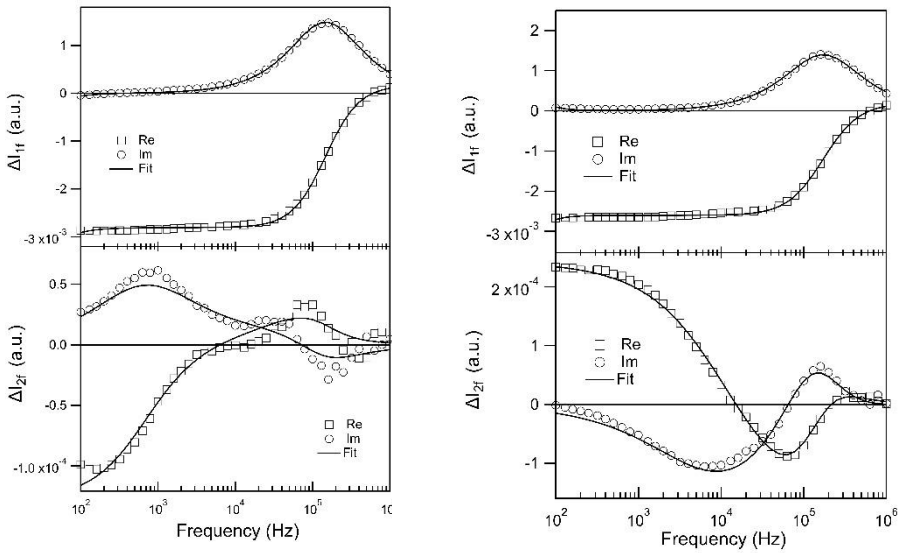

(a) (b)

Figure 5 Frequency dispersions of the linear ΔI_{1f} and second-order ΔI_{2f} responses within (a) the mid-temperature region of the SmC_α* phase at a temperature of 96.10 ℃, and (b) the low-temperature region, which is at 94.30 ℃.

Additionally, the second-order electro-optic response manifested another Debye-type relaxation mode, with its peak frequency remaining almost constant as the temperature decreased. This relaxation mode is correlated to the antiferroelectric Goldstone mode [4,6].

The contribution of the antiferroelectric Goldstone mode to Δn_a is derived from a phenomenological Landau theory [23]:

$$\Delta n_a = \frac{\varepsilon_a \xi_0^2}{4\sqrt{\varepsilon_\perp}} \left\{ c_2(\omega)\chi_{aG}(2q,0) + \mathrm{Re}\left(c_2'(\omega)\chi_{aG}(2q,2\omega)e^{i2\omega t} \right) \right\} \left(\frac{E_0}{2} \right)^2 . \qquad (10)$$

This equation provides an adequate description of the Kerr effect within the SmC_A* phase, particularly at considerable distances from the transition temperature. As predicted, the frequency dispersion of the antiferroelectric Goldstone mode adhered to a Debye-type pattern, as depicted in Figure 6(b). The formula for analyzing the frequency dispersion within the SmC_A* phase, based on Eq. (10), can be expressed as in Eq. (11):

$$\Delta I_{2f}(\omega) = \frac{A_{aG}}{1+i2\omega\tau_{aG}} \tag{11}$$

Here, τ_{aG} represents the antiferroelectric Goldstone mode relaxation time and A_{aG} is a fitting parameter related to the antiferroelectric Goldstone mode.

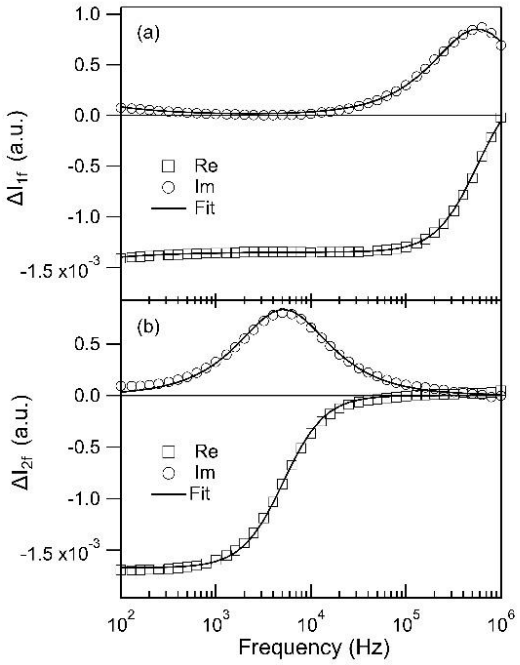

Figure 6 Frequency dispersions of the linear ΔI_{1f} (a) and the second-order ΔI_{2f} responses (b) were observed within the SmC_A* phase at $T = 92.0$ ℃.

Figure 7 displays the temperature dependency of the relaxation frequencies based on the fitted results of the second-order and linear electro-optic frequency dispersions. These frequencies are represented as $f_{r,s} = 1/2\pi\tau_s$, $f_{r,f} = 1/2\pi\tau_f$, $f_{r,aG} = 1/2\pi\tau_{aG}$. Regarding the ferroelectric mode on the high frequency side determined from the linear electro-optic response, the relaxation frequency decreased toward the transition point in the SmA phase but did not reach zero. This is natural because the lower temperature phase is not the SmC* phase but the SmC_α* phase. In the SmC_α* phase, the relaxation frequency becomes large. The relaxation frequency reached a maximum on the high temperature side of the SmC_α* phase, reached a minimum before transitioning to the SmC_A* phase, and then increased again. Immediately after the transition to the SmC_A* phase, the relaxation frequency of the ferroelectric mode became much higher. On the high temperature side of the SmC_α* phase, the relaxation frequency of the amplitude

mode determined from the second-order electro-optic response increased as it moves away from the transition point. This is the behavior we expected from the amplitude mode. Further elaboration on the relaxation frequencies surrounding the SmA–SmC$_\alpha$* phase transition can be found in earlier publications [9,15]. Notably, in the SmA phase, the soft mode is not discernible in the second-order electro-optic response. As noted in previous studies [27,29], current research efforts are directed towards adjusting specific electro-optic measurement parameters, such as α_0 and the refractive index anisotropy, n_{a0}, to potentially reveal the soft mode in the SmA phase.

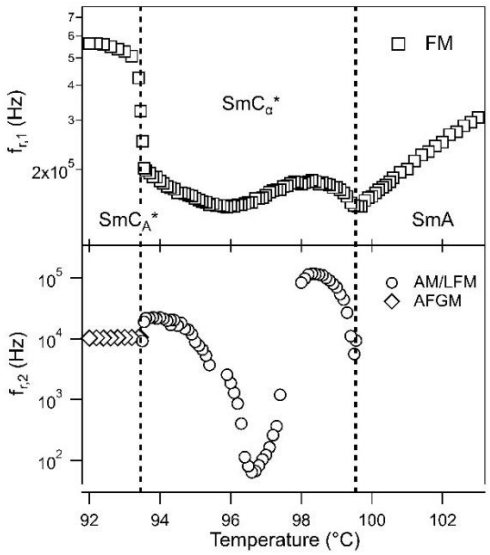

Figure 7 Temperature dependence of relaxation frequencies determined from fitting linear (fr,1: ferroelectric mode) and second-order (fr,2: amplitude/low-frequency mode, antiferroelectric Goldstone mode) nonlinear electro-optic frequency dispersions.

As the temperature decreased, a distinct trend emerged within the SmC$_\alpha$* phase. The amplitude mode relaxation frequency rose with decreasing temperature in the high temperature side of the SmC$_\alpha$* phase, but it started to gradually decline with decreasing peak intensity. The intensity further decreased and the relaxation frequency reached its minimum value around the middle of the SmC$_\alpha$* phase. From this temperature, the relaxation frequency gradually increased again. During this process of temperature change, the intensity of the amplitude mode became almost zero, so it is currently impossible to determine whether the mode that became stronger on the low temperature side was the same as the amplitude mode on the high temperature side. Therefore, this mode will be referred to as the

low-frequency mode below. In fact, the phenomenological theory only predicts that the relaxation frequency of the amplitude mode linearly increases from the SmA–SmC$_\alpha$* transition point. The above complicated behavior is probably the result of non-linearity, which is not taken into account by our phenomenological theory and is not yet clarified. As the temperature decreased, the peak intensity of the low-frequency mode decreased and at the same time the relaxation frequency increased, and before the transition to the SmC$_A$* phase, the intensity increased again and the relaxation frequency increased. The relaxation mode frequency in the SmC$_A$* phase did not change much with temperature. According to previous research results from [4,7], the mode observed in the SmC$_A$* phase is antiferroelectric Goldstone mode and therefore the relaxation mode near the SmC$_\alpha$*–SmC$_A$* phase transition point is considered to be due to the Goldstone mode. Notably, the antiferroelectric Goldstone mode maintains constant values in the SmC$_A$* phase.

It is interesting to discuss here the results of field-induced birefringence measurements on MHPOCBC with homeotropic cells, which state that there are two subphases in the SmC$_\alpha$* phase, and the phase transition between the two phases occurs in the middle of the SmC$_\alpha$* phase [30]. This can be explained by the competition of polar and non-polar biaxilities that the two subphase are SmC* and SmC$_\alpha$* phases and the phase transition is second-order, while the SmC$_A$*–SmC$_\alpha$* phase transition is first-order [31]. Electrooptical measurements showed a slowing down of the low-frequency mode in the middle of the SmC$_\alpha$* phase. However, it could not be determined at this time whether this phenomenon is related to the phase transition as mentioned above. The dielectric [21] and birefringence experiments [30,32-33] conducted in a DC field have, in fact, demonstrated that the behavior of the SmC$_\alpha$* phase varies at high and low temperatures. However, from the DSC [26], tilt angle [22], birefringence [34], and helix pitch measurements [14] in conditions without a DC field, no significant changes were observed. More research is needed regarding the slowing down of low-frequency mode observed in this study.

5 Conclusions

Linear and second-order electro-optic measurements were conducted on MHPOCBC, an antiferroelectric liquid crystal with a broad SmC$_\alpha$* phase range. The linear response showed a Debye-type dispersion, revealing temperature-dependent relaxation frequencies. The second-order response exhibited a similar Debye-type dispersion in both the SmA and the SmC$_A$* phase, whereas the SmC$_\alpha$* phase exhibited complex variations with temperature. Notably, the amplitude mode in the SmC$_\alpha$* phase revealed a marked slowing-down trend close to the SmA phase. In the low-temperature region of the SmC$_\alpha$* phase, the

relaxation frequency of the low-frequency relaxation mode increased with decreasing temperature. Furthermore, the antiferroelectric Goldstone mode, identified within the SmC_A* phase, exhibited a constant relaxation frequency across the measured temperature range. These results suggest the potential utility of nonlinear electro-optic measurement techniques in observing nonpolar modes within nonpolar phases. An ongoing investigation is underway to observe the soft mode in the SmA phase near the SmC_α* phase using nonlinear electro-optic measurement.

References

[1] Chirra, S., Iqbal, A., Lal, A., Singh, P.K., Urbańska, M., Kula, P. & Dhar, R., *Frequency Response of Dielectric Relaxation Modes in a Room Temperature Antiferroelectric Phase Liquid Crystalline Mixture*, J. Mol. Struct., **1301**, 137316, 2024.

[2] Verma, D., Punjani, V., Mohiuddin, G. & Sinha, A., *Effect of Doping Ferroelectric $BaTiO_3$ Nanoparticles on Dielectric, Electro-optical, and Ionic Properties of Antiferroelectric Bent-core Liquid Crystal*, J. Mol. Liq., **385**, 122241, 2023.

[3] Pozhidaev, E.P., Torgova, S.I. & Barbashov, V.A., *Electro-optics of Ferroelectric and Antiferroelectric Liquid Crystal Helical Nanostructures*, J. Mol. Liq., **367**, 120493, 2022.

[4] Orihara, H., Kawada, K., Yamada, N. & Ishibashi, Y., *Electro-optic Effect in an Antiferroelectric Liquid Crystal*, Mol. Cryst. Liq. Cryst. Sci. Technol. Sect. A, **303**(1), pp. 159-164,1997.

[5] Kimura, Y., Kobayashi, N. & Hayakawa, R., *Electro-optic Response of a Ferroelectric Liquid Crystal in Thick Free-standing Films*, Phys. Rev. E, **64**(1), 011705, 2001.

[6] Hiraoka, K., Takezoe, H. & Fukuda, A., *Dielectric Relaxation Modes in the Antiferroelectric Smectic C_A* Phase*, Ferroelectrics, **147**(1), pp. 13-25, 1993.

[7] Hiraoka, K., Uematsu, Y., Takezoe, H. & Fukuda, A., *Molecular Fluctuations in Smectic Phases Possessing Antiferroelectric Ordering*, Japan. J. Appl. Phys., **35**(12R), pp. 6157-6161, 1996.

[8] Kimura, Y., Nagata, T. & Hayakawa R., *Nonlinear Electro-optical Spectroscopy of Ferroelectric Liquid Crystals*, Ferroelectrics, **213**(1), pp. 81-90, 1998.

[9] Kimura, Y. & Hayakawa, R., *Nonlinear Electrooptical Relaxation Spectra of Ferroelectric and Antiferroelectric Liquid Crystals*, Mol. Cryst. Liq. Cryst. Sci. Technol. Sect. A, **328**(1), pp. 83-92, 1999.

[10] Fukuda, A., Takanishi, Y., Isozaki, T., Ishikawa, K. & Takezoe, H., *Antiferroelectric Chiral Smectic Liquid Crystals*, J. Mater. Chem, **4**(7), pp. 997-1016, 1994.

[11] Takezoe, H., Gorecka, E. & Čepič, M., *Antiferroelectric Liquid Crystals: Interplay of Simplicity and Complexity*, Rev. Mod. Phys., **82**(1), pp. 897-937, 2010.

[12] Fukuda, A., Vij, J.K. & Takanishi, Y., *Variety of Subphase Emerging Sequences, the Frustration of Three Main Phases, SmC_A*, SmC*, and SmA, and the Long-range Interlayer Interactions*, Phys. Rev. E, **104**(1), 014705, 2021.

[13] Mach, P., Pindak, R., Levelut, A.M., Barois, P., Nguyen, H.T., Huang, C.C. & Furenlid, L., *Structural Characterization of Various Chiral Smectic- C Phases by Resonant X-Ray Scattering*, Phys. Rev. Lett., **81**(5), 1015, 1998.

[14] Cady, A., Han, X.F., Olson, D.A., Orihara, H. & Huang, C.C., *Optical Characterization of a Nanoscale Incommensurate Pitch in a New Liquid-crystal Phase*, Phys. Rev. Lett., **91**(12), 125502, 2003.

[15] Bourny, V., Fajar, A. & Orihara, H., *Observation of the Soft Mode in the Sm-C_α* Phase*, Phys. Rev. E, **62**(5), pp. R5903- R5906, 2000.

[16] Bourny, V., Fajar, A. & Orihara, H., *Linear and Nonlinear Electro-optic Studies of the Smectic-A-Smectic-C_α* Phase Transition*, Mol. Cryst. Liq. Cryst. Sci. Technol. Sect. A, **364**(1), pp. 373-380, 2001.

[17] Orihara, H., Fajar, A. & Bourny, V., *Observation of the Soft-mode Condensation in the Sm-A-Sm-C_α* Phase Transition by Nonlinear Dielectric Spectroscopy*, Phys. Rev. E, **65**(4), 040701, 2002.

[18] Fajar, A., Murai, H. & Orihara, H., *Nonlinear Dielectric Spectroscopy in the Smectic-A-smectic-C_α* Phase Transition*, Phys. Rev. E**, 65**(4), 041704, 2002.

[19] Kimura, Y., Isono, H. & Hayakawa, R., *Nonlinear Dielectric Response of Antiferroelectric Liquid Crystals in the Smectic C_α* Phase*, Eur. Phys. J. E, **9**, pp. 3-13, 2002.

[20] Lagerwall, J.P.F., *Demonstration of the Antiferroelectric Aspect of the Helical Superstructures in Sm-C*, Sm-C_α*, and Sm-C_A* Liquid Crystals*, Phys. Rev. E, **71**(5), 051703, 2005.

[21] Hiraoka, K., Takanashi, Y., Takezoe, H., Fukuda, A., Isozaki, T., Suzuki, Y. & Kawamura, I., *Dielectric Behavior and the Devil's Staircase in the SmC_α* Phase of an Antiferroelectric Liquid Crystal, 4-(1-methylheptyloxycarbonyl)phenyl 4'-octylcarbonyloxybiphenyl -4-carboxylate*, Jpn. J. Appl. Phys., **31**(10R), pp. 3394-3998, 1992.

[22] Isozaki, T., Hiraoka, K., Takanishi, Y., Takezoe, H., Fukuda, A., Suzuki, Y. & Kawamura, I., *Conoscopic Study of the $S_{C\alpha}$* Phase and the Devil's Staircase in an Antiferroelectric Liquid Crystal*, Liq. Cryst., **12**(1), pp. 59-70, 1992.

[23] Orihara, H. & Ishibashi, Y., *Electro-optic Effect and Third-Order Nonlinear Dielectric Response in Antiferroelectric Liquid Crystals*, J. Phys. Soc. Jpn., **64**(10), pp. 3775-3786, 1995.

[24] Musevic, I., Blinc, R. & Zeks, B., *The Physics of Ferroelectric and Antiferroelectric Liquid Crystals*, Singapore: World Scientific, 2000.

[25] Bourny, V., Pavel, J., Lorman, V., & Nguyen, H.T., *Phase Transitions in the Antiferroelectric Liquid Crystal C8 Tolane Determined by Dielectric and Electrooptical Measurements*, Liq. Cryst., **27**(5), pp. 559-566, 2000.

[26] Isozaki, T., Suzuki, Y., Kawamura, I., Mori, K., Nakamura, N., Yamamoto, N., Yamada, Y., Orihara, H. & Ishibashi, Y., *Successive Phase Transitions in Antiferroelectric Liquid Crystal 4-(1-methylheptyloxycarbonyl)phenyl 4'-octylcarbonyloxybiphenyl-4-carboxylate (MHPOCBC)*, Jpn. J. Appl. Phys.**,** **30**(9A), L1573, 1991.

[27] Fajar, A., Bourny, V. & Orihara, H., *Fluctuation-induced Kerr Effect Near the Smectic-A-smectic-C_α* Phase Transition*, Mol. Cryst. Liq. Cryst. Sci. Technol. Sect. A, **366**(1), pp. 653-660, 2001.

[28] Fajar, A., Orihara, H., Bourny, V., Pavel, J. & Lorman, V., *Electro-optic Measurement in the Vicinity of SmA-SmC_α* Phase Transition of an Antiferroelectric Liquid Crystal*, Japan. J. Appl. Phys., **39**(2B), L166, 2000.

[29] Fajar, A., Bourny, V. & Orihara, H., *Nonlinear Electrooptical Measurements in the Smectic-C_α* Phase*, Jpn. J. Appl. Phys., **42**(1R), pp. 182-185, 2003.

[30] Shtykov, N.M., Chandani, A.D.L., Emelyanenko, A.V., Fukuda, A. & Vij, J. K., *Two Kinds of Smectic-C_α* Subphases in a Liquid Crystal and Their Relative Stability Dependent on the Enantiomeric Excess as Elucidated by Electric-field-induced Birefringence Experiment*, Phys. Rev. E, **71**(2), 021711, 2005.

[31] Emelyanenko, A.V., Fukuda, A. & Vij, J.K., *Theory of the Intermediate Tilted Smectic Phases and Their Helical Rotation*, Phys. Rev. E, **74**(1), 011705, 2006.

[32] Takanishi, Y., Iida, A., Yadav, N., Chandani Perera, A.D.L., Fukuda, A., Osipov, M.A. & Vij, J.K., *Unexpected Electric-field-induced Antiferroelectric Liquid Crystal Phase in the SmC_α* Temperature Range and the Discrete Flexoelectric Effect*, Phys. Rev. E, **100**(1), 010701, 2019.

[33] Orihara, H., Naruse, Y., Yagyu, M., Fajar, A. & Uto, S., *Electric-field-temperature Phase Diagram of an Antiferroelectric Liquid Crystal*, *Phys. Rev. E*, **72**(4), 040701, 2005.

[34] Škarabot, M., Čepič, M., Žekš, B., Blinc, R., Heppke, G., Kityk, A.V. & Muševič, I., *Birefringence and Tilt Angle in the Antiferroelectric, Ferroelectric, and Intermediate Phases of Chiral Smectic Liquid Crystals*, Phys. Rev. E, **58**(1), pp. 575-584, 1998.